The roles of CEN2 and DLC8a in apical secretory organelles discharge of toxoplasma gondii

Lentini, Gaëlle; Dubois, David Jean; Maco, Bohumil; Soldati-Favre, Dominique; Frenal, Karine

How to cite

LENTINI, Gaëlle et al. The roles of CEN2 and DLC8a in apical secretory organelles discharge of toxoplasma gondii. In: Traffic, 2019. doi: 10.1111/tra.12673

This publication URL: https://archive-ouverte.unige.ch/unige:119691
Publication DOI: 10.1111/tra.12673

The roles of CEN2 and DLC8a in apical secretory organelles discharge of *Toxoplasma gondii*

Gaëlle Lentini, David J. Dubois, Bohumil Maco, Dominique Soldati-Favre[1§] and Karine Frénal[1,2§]

Affiliations

[1]Department of Microbiology and Molecular Medicine, CMU, University of Geneva, 1 Rue Michel-Servet, CH-1211 Geneva 4, Switzerland

[2]Microbiologie Fondamentale et Pathogénicité University of Bordeaux, CNRS UMR 5234, 146 Rue Léo Saignat, 33076 Bordeaux Cedex, France

[§]Correspondence to: dominique.soldati-favre@unige.ch, karine.frenal@u-bordeaux.fr

This article has been accepted for publication and undergone full peer review but has not been through the copyediting, typesetting, pagination and proofreading process which may lead to differences between this version and the Version of Record. Please cite this article as doi: 10.1111/tra.12673

Running Title: Role of CEN2 and DLC8a in organelle discharge

Synopsis:

CEN2 and DLC8a are associated with tubulin-rich structures in *Toxoplasma gondii,* playing pivotal roles at the apical pole of the parasite. CEN2 is essential for microneme exocytosis supporting motility, invasion and egress. DLC8a appears responsible for sustained microneme replenishment in addition to its role in rhoptry positioning and discharge. Overall, DLC8a acts as an important player in trafficking and apical anchoring of secretory organelles, while CEN2 acts as a gateway for organelle exocytosis, possibly via Ca^{2+}-dependent contractions.

Abstract

To efficiently enter host cells, apicomplexan parasites such as *Toxoplasma gondii* rely on an apical complex composed of tubulin-based structures as well as two sets of secretory organelles named micronemes and rhoptries. The trafficking and docking of these organelles to the apical pole of the parasite is crucial for the discharge of their contents. Here we describe two proteins typically associated with microtubules, Centrin 2 (CEN2) and Dynein Light Chain 8a (DLC8a), that are required for efficient host cell invasion. CEN2 localizes to four different compartments, and remarkably, conditional depletion of the protein occurs in stepwise manner, sequentially depleting the protein pools from each location. This phenomenon allowed us to discern the essential function of the apical pool of CEN2 for microneme secretion, motility, invasion and egress. DLC8a localises to the conoid, and its depletion also perturbs microneme exocytosis in addition to the apical docking of the rhoptry organelles, causing a severe defect in host cell invasion. Phenotypic characterization of CEN2 and DLC8a indicates that while both proteins participate in microneme secretion, they likely act at different steps along the cascade of events leading to organelle exocytosis.

Keywords

Apicomplexa, *Toxoplasma gondii,* centrin, dynein light chain, conoid, microneme, exocytosis, rhoptries, motility, invasion, egress, annuli

Introduction

Microtubules are filamentous tubulin heteropolymers found in all eukaryotic cells. They provide a framework that is essential for the maintenance of cellular architecture and shape. In addition to their structural role, microtubules are also involved in a wide variety of cellular processes such as chromosome segregation, intracellular transport of organelles and vesicles, as well as ciliary and flagellar motility (for a review see [1]). Microtubules originate from the microtubule organizing centre (MTOC) which is the site for coordinated microtubule nucleation. Remarkably, the obligate intracellular parasite *Toxoplasma gondii* harbours two MTOCs from which emerge distinct populations of microtubules. The centrocone is a unique spindle compartment of the nuclear envelope that is associated with centrosomes and is responsible for chromosome segregation during closed mitosis [2]. It has been implicated in daughter cell budding, division of the Golgi apparatus and the inheritance of a non-photosynthetic plastid-like organelle called the apicoplast [3–5]. The second MTOC is non-centrosomal and consists of a ring-shaped tubulin structure, positioned at the apex of the parasite, referred to as the apical polar ring (APR). Twenty-two subpellicular microtubules emerge from the APR and elongate along two-thirds of the parasite body. They form a cytoskeletal basket that supports the pellicle of the parasite and maintains its shape and rigidity. Present in all alveolates, the pellicle is composed of a unique triple lipid bilayer, which is made of the plasma membrane apposed to flattened membranous vesicles called the inner membrane complex (IMC). This is underlined by an elaborate network of intermediate filament-like alveolins [6]. Anchored to the APR, the conoid is composed of a tightly-packed spiral of atypical tubulin polymer fibers [7] with a pair of intraconoidal microtubules at its centre and two pre-conoidal rings at the top. The conoid is a motile structure which is retracted inside the cell body in intracellular parasites but extrudes through the APR in extracellular parasites due to a rise in intracellular calcium (Ca^{2+}) levels [8].

Besides these tubulin structures, the apical complex of *T. gondii* harbours two types of regulated secretory organelles, the micronemes and the rhoptries, that are secreted sequentially during host cell invasion. Micronemes contain, amongst other proteins, adhesins that are associated with the parasite plasma membrane post-exocytosis and play a role in motility, invasion and egress [9]. Rhoptries are elongated organelles composed of a bulbous region and a neck region containing ROPs and RONs proteins, respectively. Once secreted, a complex of RON proteins is inserted into the cytoplasmic face of the host cell plasma membrane and interacts with the microneme protein AMA1 (apical membrane antigen 1) at the parasite surface. This establishes a firm anchor, termed the moving circular junction, through which the parasite can propel itself into the host cell [10].

Proper apical positioning and secretion of these two secretory organelles are crucial for successful invasion and hence the survival of *T. gondii*. Micronemes are typically organized like a crown around the APR and are associated with the subpellicular microtubules [11,12]. The rhoptries are clustered together just beneath

the conoid except for the one or two that are primed for secretion and are observed with their neck inserted into the conoid, possibly by docking to the intraconoidal microtubules [13,14]. The acylated ARO protein is anchored to the cytoplasmic face of the rhoptry membrane and is essential for the apical positioning and clustering of the organelles [15–18]. The integrity of the APR and subpellicular microtubules is crucial for microneme trafficking and anchoring to the apical pole of the parasite [12].

Both sets of secretory organelles appear to be secreted at the apex of the parasite [19] in response to elevated intracellular Ca^{2+}. Microneme exocytosis depends on a pleckstrin-homology domain-containing protein (APH) that is anchored by acylation to the surface of micronemes and is able to sense phosphatidic acid (PA) [20–22]. Ultimately, binding of APH to PA triggers a membrane fusion event that releases the microneme content via a hypothetical SNARE-like complex involving DOC2.1 [23]. The signalling cascade leading to rhoptry secretion is still unknown, nevertheless a recent study showed that parasites conditionally depleted for FER2, a Ca^{2+} sensor belonging to the ferlin family, are unable to discharge the rhoptries. This suggests that rhoptry secretion might also be driven by Ca^{2+} signalling [24]. Even though valuable advances have been made towards a better understanding of the rhoptry and microneme membrane fusion mechanisms, little is known about the docking and transport of these secretory organelles to the site of fusion at the tip of the parasite. Secretion of both organelles is thought to occur via the conoid, but most of the conoidal proteins studied so far have been implicated in conoid stability [12,25,26]. Only depletion of the polar ring associated protein, RNG2, has been reported to impact modestly on microneme exocytosis [27].

Both *T. gondii* centrin 2 (CEN2) and dynein light chain 8a (DLC8a) localize to the apical complex and are predicted to be essential based on the fitness score obtained from a CRISPR-Cas9 genome wide knockout screen [28]. Centrins are a group of highly conserved eukaryotic Ca^{2+} binding phosphoproteins that mediate Ca^{2+}-dependent contraction of the ring structures typically associated with centrioles or flagellum [29,30]. In *T. gondii*, CEN2 is found at the centrosome, the peripheral annuli, the pre-conoidal ring and the basal cup of the parasites [31]. Intriguingly, the apical complex of the *T. gondii* tachyzoite is believed to originate from a repurposed flagellum [32]. This could suggest that the apically localized CEN2 has flagellar origins. For example, in the flagellated green algae *Chlamydomonas reinhardtii*, centrins have been documented to contribute to Ca^{2+}-mediated contraction and flagellum excision [33]. Intriguingly, the peripheral annuli are enigmatic structures that have been described only in *T. gondii*. They consist of six circles positioned at the lower edge of the apical cap. The functional relevance of these annuli is presently unknown and only two markers have been described, namely, CEN2 and the peripheral annuli protein 1 (PAP1) [34]. The pool of CEN2 localizing to the basal cup is involved in the constriction of the basal pole, a non-essential process that occurs at the end of division [35]. The role of CEN2 at the other locations is unknown.

DLC8a belongs to a family of cytoskeletal motor proteins that form a functional complex with the cytoplasmic dynein

heavy chains, intermediate chains and light intermediate chains. This complex transports cargoes, such as vesicles and organelles, along microtubules over long distances in the cytoplasm (for a review see [36]). DLC8 is found in all eukaryotes studied so far including those lacking cytoplasmic dynein heavy chains such as higher plants or red algae [37]. Among the four DLC8 proteins expressed by *T. gondii* [38], DLC8a is the only one that has been proposed to be important for the tachyzoite lytic cycle [28]. One of the cytoplasmic dynein heavy chains conserved across the phylum of Apicomplexa is also important for parasite fitness suggesting that it might form a motor complex with DLC8a (**Table S1**) [37]. When expressed as a second copy, DLC8a localizes to the apical tip, spindle poles, centrosome and basal ring of the parasites [31], whereas endogenously C-terminal tagged DLC8a localizes only to the apical cap [38].

Here we have embarked on a phenotypic analysis of these two conserved apicomplexan proteins typically associated with microtubules. By conditionally controlling CEN2 expression, we have identified its subcellular localization-dependent role in microneme secretion that ensures motility, invasion and egress. CEN2 also appears to be implicated in the integrity of the peripheral annuli. In contrast, DLC8a contributes predominantly to invasion by sustaining successive rounds of microneme secretion and by properly anchoring the rhoptries to the apical complex.

Results

Gradual depletion of CEN2 results in distinct phenotypes linked to its multiple localization

C-terminal tagging of CEN2 with yellow fluorescent protein (YFP) at the endogenous locus revealed punctate structures associated with the centrosome, the pre-conoidal ring, the peripheral annuli and the basal cup of the parasite [39]. CEN2 at the posterior pole participates in the basal constriction of the parasite in association with the myosin motor MyoJ, a function that has been shown to be dispensable for parasite survival [35]. Considering the highly negative fitness score for CEN2 mutants reported in a *T. gondii* genome-wide screen [28], we postulated that CEN2 carried important additional functions at its other locations. To address this point, we dissected its role using a Tet-inducible CEN2-YFP parasite line (CEN2-iKD) [35]. Immunofluorescence assays (IFA) revealed that CEN2 depletion occurred in a stepwise manner (**Figure 1A**). First, a loss of CEN2 was observed 24h after ATc treatment at the peripheral annuli and the conoid. Depletion of CEN2 from the basal cup occurred only at 48h (**Figure 1A,** yellow arrowheads). The pool of CEN2 associated with the centrosomes was the last to be affected and was still weakly detectable after 72h of ATc treatment (**Figure 1A,** white arrows).

We assessed the effect of long-term depletion of CEN2 by evaluating the viability of the parasites on plaque assay (**Figure 1B**). Every 48h, the parasites accomplish an entire lytic cycle ending by egressing from the infected cells and invading the neighbouring ones. Over a period of 7 days, areas of lysis became visible on the monolayer, recapitulating several successful lytic cycle rounds. The monolayer infected with CEN2-depleted

parasites appeared almost intact, reflecting the deleterious consequence of CEN2 depletion on parasite survival (**Figure 1C**). Taking advantage of the sequential loss of CEN2, we evaluated the impact of CEN2 depletion from its various locations over time. To assess the role of CEN2 in division with regards to its centrosomal localization, CEN2-iKD parasites were grown in the presence of ATc for 72h. These parasites replicated in a manner comparable to the treated parental strain (control) (**Figure 1D**). We then evaluated the synchronicity of division at 48h of ATc treatment when the basal pool of CEN2 was depleted. In this assay, all the parasites within the same vacuole divided in a synchronous fashion, indicating that CEN2 does not play a role in the intravacuolar connection between parasites (**Figure S1A**). These observations reveal that CEN2 at the centrosome and basal pole is not critical for parasite proliferation.

The function of CEN2 at the apical pole of the parasite was assessed by phenotyping the parasites after 48h of ATc treatment. At that time, the pools of CEN2 at the apical tip and annuli are undetectable. CEN2 depleted parasites were impaired in their ability to invade host cells by 85% compared to control parasites (**Figure 2A**). We observed a comparable defect in the ability of the parasites to egress from the infected host cell (**Figure 2B**). Analysis of parasite motility by video microscopy revealed that 80% of CEN2 depleted parasites were non-motile versus 40% in the control strain (**Figure 2C and S1B**). Among the remaining motile parasites, the three types of movement, helical, circular and stationary twirling, were observed (**Figure S1C**). Successful invasion, egress and motility rely on adhesins that are released to the parasite surface upon microneme exocytosis (**Figure 1B**). As CEN2 depletion led to a defect in these three processes, we evaluated the ability of these parasites to secrete their micronemes. CEN2-depleted parasites showed a lower basal level of microneme secretion, compared to both control and untreated parasites, and a complete inability to respond to ethanol, a chemical inducer of microneme exocytosis (**Figure 2D**). In accordance with the defect in microneme exocytosis, parasite attachment to host cells was severely impaired, with attachment efficiency dropping by 70% between the control and CEN2 depleted parasites (**Figure 2E**). The absence of CEN2 did not affect the morphology and the subcellular distribution of micronemes and rhoptries (**Figure 2F**). Moreover, induced conoid protrusion was not impaired upon CEN2 depletion (**Figure S1D**). Overall, these results point to a key role for CEN2 in microneme exocytosis that ensures motility, attachment, invasion, and egress.

Depletion of CEN2 destabilizes the peripheral annuli

At the parasite apex, CEN2 localizes to the peripheral annuli, a structure of unknown function for which only one other marker has been described to date, the peripheral annuli protein 1 (PAP1) [34]. Using super-resolution microscopy by stimulated emission depletion (STED), we confirmed that endogenously tagged PAP1 specifically localizes to the peripheral annuli (**Figure 3A**). Moreover, 3D reconstruction of PAP1 and CEN2 staining indicated that PAP1 forms a ring-shaped structure surrounding CEN2-YFP (**Figure 3B**). To evaluate if the loss of PAP1 affected CEN2 localization, we generated PAP1-KO transgenic parasites in the

CEN2-iKD background (PAP1-KO/CEN2-iKD, **Figure S2A**). In the absence of PAP1, CEN2-YFP still localized correctly at the peripheral annuli (**Figure 3C**) and did not appear to be degraded (**Figure 3D**). Moreover, deletion of PAP1 did not affect the fitness of the parasites which were still able to accomplish their lytic cycle (**Figure 3E**). PAP1-KO parasites were able to invade, replicate and egress as efficiently as the control (**Figure S2B-D**).

Reciprocally, we asked if the loss of CEN2 could affect the structure of the peripheral annuli. Despite several attempts, we were unable to visualise PAP1 in CEN2-iKD parasites. Instead, we used a novel marker of the peripheral annuli, TGGT1_230340, which we identified by mass spectrometry on a biotin-based proximity-labelling (BioID) experiment using SAS6L, a protein found above the conoid [32] (**Dataset S1**). Epitope tagging of TGGT1_230340 at the endogenous locus revealed that this protein specifically localized to the peripheral annuli and we therefore named it PAP2. PAP1 and PAP2 are largely conserved in the coccidian-subgroup of Apicomplexa (**Table S1**) but the two proteins do not share any obvious sequence homology. PAP1 contains two coiled-coil domains and a putative intermediate filament-binding trichohyalin-like domain with 11 repeats of a 33 amino-acid stretch (**Figure S3A**). PAP2 is predicted to possess armadillo repeats and a coiled-coil domain (**Figure S3B and C**).

PAP2 localization by STED microscopy revealed a labelling that resembles that of PAP1, with a ring shape structure localized exclusively to the six peripheral annuli of the parasite (**Figure 3F)**. A 3D surface reconstruction of PAP2 labelling indicated that it surrounds CEN2-YFP at each annulus, suggestive of a multiple layered structure at the peripheral annuli (**Figure 3G and Movie S1)**. The peripheral annuli have been shown to be resistant to detergent extraction, probably because of their association with the subpellicular cytoskeleton [31]. To test if these structures are connected with the subpellicular microtubules, we treated parasites for 24h with 0.5 nM oryzalin, an herbicide known to bind and inhibit plant microtubule polymerization without affecting mammalian microtubules. In *T. gondii*, 0.5 nM oryzalin is known to efficiently disrupt the subpellicular microtubules without causing aberrant cell division [40] (**Figure 4A**, ΔKU80). Under these conditions, the three markers of the peripheral annuli remained unaffected suggesting that peripheral annuli protein localization is not dependent on the subpellicular microtubules (**Figure 4A**).

In order to follow the peripheral annuli in the absence of CEN2, we endogenously tagged PAP2 at its C-terminus in CEN2-iKD parasites (CEN2-iKD/PAP2-3Ty). PAP2 distribution was clearly affected by the depletion of CEN2. Up to 70% of the parasites presented either a fainter PAP2 signal, an aberrant PAP2 localization, or a reduced number of PAP2 positive annuli per parasite. This contrasted with the six peripheral annuli homogenously observed in control parasites (**Figure 4B**). Concordantly, the level of PAP2-3Ty protein assessed by western blot, was significantly decreased upon depletion of CEN2 (**Figure 4C**). Despite the fact that PAP2 depletion was predicted to have a low impact on parasite fitness (fitness score of -1.14 [28]), we were unable to generate a PAP2-KO parasite line to determine if the absence of PAP2 had an impact on the localization of CEN2 or PAP1 at the

peripheral annuli. In conclusion, the peripheral annuli are stable in the absence of the subpellicular microtubules, whereas the depletion of CEN2 appears to be important for the localization of PAP2.

DLC8a is associated with tubulin-rich structures

DLC8a has been previously reported to localize to structures that appose with structures exhibiting CEN2 labelling, suggesting that these two proteins might, in part, share a similar function. When expressed as a second copy, DLC8a localized to the polar ring, the conoid, the spindle poles, the centrosome and the basal ring [31]. In another study, a C-terminal tagged version of DLC8a was reported to localize solely at the apical cap [38]. To investigate DLC8a function, we generated an inducible knockdown cell line, MycDLC8a-iKD, by exchanging the endogenous promoter with the ATc regulatable promoter that expressed an N-terminal Myc epitope-tagged DLC8a protein (Myc-DLC8a; **Figure S4A and B**). In intracellular parasites, Myc-DLC8a localized to the parasite centrosome and at the apical cap with a stronger signal at the APR (**Figure 5A**). At the centrosome, DLC8a colocalized with the CEN1 and CEN2 labelling (**Figure 5A - top panels**). At the apical pole, Myc-DLC8a was detected at a site more apical than the micronemes and the rhoptries (**Figure 5A - lower panels**). In extracellular parasites, the protein localised on the top of the retracted conoid, while upon treatment with the Ca^{2+} ionophore A23187 (an inducer of conoid protrusion), Myc-DLC8a labelling was detected on the entire extruded conoid (**Figure 5B**) as previously reported by immuno-electron microscopy [31].

In intracellular parasites treated with 0.5 nM oryzalin, Myc-DLC8a was still detected at the apical cap of the parasite, indicating that its localization is unaffected by the absence of the subpellicular microtubules (**Figure 5C**).

TgDLC8a drives microneme secretion, required for parasite attachment

As with CEN2, assessing the functional roles of DLC8a is challenging because it resides at multiple sites and thus several phenotypes might overlap. In MycDLC8a-iKD parasites, Myc-DLC8a levels were undetectable after 48h of ATc treatment using both IFA and western-blot (**Figures 5D and E**). Parasites depleted of DLC8a generated smaller lysis plaques than control parasites, indicative of a defect in one or multiple steps of the lytic cycle (**Figure 5F**). The role of DLC8a at the centrosomes was evaluated by scoring the number of parasites per vacuole after 60h of ATc treatment. In this assay, no delay in replication was observed (**Figure 5G**).

In contrast, DLC8a plays a critical role at the apical pole of the parasite, with less than 10% of DLC8a-depleted parasites being able to invade compared to the control (**Figure 6A**). To further dissect the phenotype, microneme secretion was assayed following triggering by either ethanol or BIPPO, a phosphodiesterase inhibitor [41]. DLC8a-depleted parasites failed to secrete MIC2 above basal levels in response to both stimulations (**Figure 6B**). This defect was also observed for the secretion of two other microneme proteins, AMA1 and MIC8 (**Figure S4C**). However, upon DLC8a depletion, the micronemes were still properly positioned at the apical pole, suggesting a role for DLC8a in the cascade of events leading to microneme exocytosis and not in the trafficking or

apical positioning of the organelles (**Figure 6C**). The basal level of microneme secretion observed in DLC8a-depleted parasites seemed insufficient to promote efficient parasite attachment and invasion into the host cell (**Figure 6D**), although it supported egress and motility (**Figures 6E, 6F and S4D**). Overall, depletion of DLC8a strongly impact invasion and microneme secretion but only moderately affect motility, egress and attachment.

Depletion of TgDLC8a results in aberrant positioning of the rhoptries impacting on their discharge

DLC8a-depleted parasites exhibited a severe invasion defect, with motility and egress being unexpectedly normal. This suggested an additional role for DLC8a in rhoptry function. In these parasites, IFAs performed with antibodies to the rhoptry membrane marker, ARO, demonstrated a typical apical signal for the rhoptries, but also revealed the unexpected presence of filamentous structures all over the parasite body – as previously reported in ARO depleted parasites [16] (**Figure 7A**). This abnormal staining for the rhoptries was confirmed with anti-RON9 and anti-ROP7 antibodies. ROP7 labelling showed a similar filamentous pattern as ARO labelling, whereas RON9 appeared more punctiform. Both ROP7 and RON9 overlap with ARO, indicating that they are still associated with rhoptry material despite the fact that the rhoptry sub-compartments cannot be clearly delineated.

The ultrastructure of the DLC8a-depleted parasites in several vacuoles was analysed by transmission electron microscopy (TEM) (**Figure S5A-C**) and focussed ion beam milling combined with scanning electron microscopy (FIB-SEM) (**Figure 7B-D** and **Movie S2**). No noticeable defect on the morphology of the apical pole was observed. The conoid appeared normal with rhoptries properly docked to the apex (**Figure S5A-B**) and the typical crown of micronemes at its base. (**Figure S5C)**. However, in several sections, some mature rhoptries did not cluster with the apical ones but rather were dispersed in the cytoplasm (one to five rhoptries per parasite in the serial sections analysed) (**Figures 7B-D and Figure S5B, yellow coloured letters**). FIB-SEM serial sections were used to perform 3D reconstruction of one representative DLC8a-depleted parasite (**Figure 7E**). This 3D image confirmed that several mature rhoptries were dispersed within the parasite, while others were properly clustered apically with one docked into the conoid.

Considering the presence of apically docked rhoptries and yet the severe invasion defect observed in DLC8a-depleted parasites, we investigated the ability of the rhoptries to discharge their content. ROP16 is a parasite effector protein secreted into the host cell to modulate the host immune response by phosphorylating the protein STAT6 [42]. Here the secreted ROP16-dependent level of STAT6 phosphorylation (STAT6-P) was used to quantify rhoptry discharge. Since DLC8a-depleted parasites already presented an attachment defect, STAT6-P positive cells were normalized to the number of attached parasites instead of the number of host cell nuclei. In the absence of DLC8a, the parasites lost 50% of their ability to discharge the rhoptries compared to control parasites (**Figures 7F**). Distinctly, DLC8a-depleted extracellular parasites showed no defect in BIPPO-stimulated conoid protrusion (**Figure S5D**).

Taken together these results highlight a dual role of DLC8a in stimulating microneme exocytosis and in proper apical positioning of the rhoptries, both of which are critical for successful host cell invasion.

CEN2 and DLC8a are distinct mediators of organelle exocytosis

We showed that CEN2 and DLC8a were found in apposed structures and that both proteins were involved in microneme exocytosis. This led us to investigate a potential interaction between them. We endogenously tagged CEN2 in MycDLC8a-iKD parasites (CEN2-YFP/MycDLC8a-iKD). Depletion of DLC8a following ATc treatment did not impact the localization (**Figure 8A**) or the expression level of CEN2-YFP (**Figure 8B**). Reciprocally, we transiently expressed eGFP-DLC8a [31] in CEN2-iKD parasites. In absence of CEN2-YFP (following ATc treatment), the level of eGFP-DLC8a remained unaffected (**Figure 8C**). To rule out any physical interaction between CEN2 and DLC8a, we performed co-immunoprecipitation followed by mass spectrometry analysis of either CEN2-YFP or Myc-DLC8a immunoprecipitates (**Dataset S2**). In these experiments, CEN2 was not found in Myc-DLC8a immunoprecipitates and DLC8a was not found in CEN2-YFP immunoprecipitates. These experiments confirmed that the two proteins do not directly interact and likely act independently on the cascade of events leading to microneme exocytosis. Relevantly, PAP2 was found in the mass spectrometry results of CEN2-YFP pull-down, supporting our previous observations and suggesting that the two proteins are associated at the peripheral annuli (**Figures 4B and C**).

Discussion

In this study, we dissected the roles of DLC8a and CEN2, two conserved proteins across the Apicomplexa that are linked to several microtubule-based structures (**Table S1**). We showed that both proteins fulfill multiple, essential tasks in *T. gondii* parasites. While DLC8a deletion was achieved with concomitant disappearance of the protein from the centrosomes, the apical cap and the polar ring, the knockdown of CEN2 gene expression resulted in a stepwise disappearance of the protein from its multiple locations. The pools of CEN2 associated with the pre-conoidal rings and the peripheral annuli were the first to be depleted, whereas depletion of CEN2 from the basal cup and the centrosomes occurred later. The differential kinetics of CEN2 depletion illustrates the peculiar mechanism of division of *T. gondii*, with the apical complex made *de novo* for the two daughter cells at each division cycle, while the centrosome is a highly stable structure that duplicates and is inherited from the mother [43]. The pool of CEN2 associated with the basal cup, a structure also made *de novo* for each daughter cell, is lost at an intermediate rate. The fact that CEN2 at this location disappears later than in the other *de novo* structures could be partly due to a recycling process from the basal pole of the mother, as previously shown for IMC proteins [44].

The parasites depleted of CEN2 divide normally, suggesting that either the residual amount of CEN2 observed at the centrosome is sufficient to support division or that CEN2 carries a non-essential function at this location. In favour of the latter hypothesis, the presence of two other

centrins, CEN1 and CEN3, which localize to the centrosome [31] and are likely essential for tachyzoite survival [28], might assure proper eukaryotic chromosome segregation. Both CEN2 and MyoJ are involved in the posterior constriction of the parasites, while MyoI is responsible of the intravacuolar connection [35]. In contrast to MyoJ/MyoI depletion, the absence of CEN2 does not impact the intravacuolar connection, since CEN2-depleted parasites still divide synchronously. Consequently, the intravacuolar connection is independent of the basal constriction but requires the presence of MyoJ and MyoI.

Remarkably, both CEN2 and DLC8a are implicated in microneme exocytosis, although the phenotypic consequences of their depletion are distinct. CEN2 ensures sufficient microneme secretion to support motility, attachment, invasion and egress. Microneme exocytosis likely occurs after the passage of the organelles through the conoid, and we postulate a role for CEN2 at the pre-conoidal rings in this process. Alternatively, CEN2 could play a more active role either by triggering the contraction of the pre-conoidal rings that might be needed for microneme secretion or, as a phosphoprotein, by functioning in the signalling cascade leading to microneme exocytosis [45] without affecting conoid protrusion. In this context, centrins have been reported in *Paramecium* to buffer Ca^{2+} and to down-regulate the signal after stimulation of exocytosis [46]. Additionally, in vertebrate photoreceptor cells, a centrin complex is believed to block protein and small molecule passage in the presence of Ca^{2+} [47].

In contrast to CEN2 depletion, the absence of DLC8a impacts microneme secretion in a subtler manner, since motility, attachment and egress were not abrogated. While the existence of at least two distinct subpopulations of micronemes has been reported [48], DLC8a-depleted parasites are uniformly unable to secrete MIC2, AMA1 and MIC8, ruling out a selective role of DLC8a on one subpopulation of organelles. Microneme secretion occurs in waves in response to fluctuation in intracellular Ca^{2+}, suggesting that small groups of micronemes might be transferred sequentially to the conoid [8]. In accordance with this model, subsets of micronemes are localized underneath the APR of the parasite while others are found more basally. DLC8a-depleted parasites appear unable to sustain the successive waves of exocytosis that may be necessary to support the ultimate step of the entry process. In such a scenario, a population of micronemes that are already apically localized and primed for secretion would be secreted, while microneme replenishment for subsequent secretion would be impaired due to a defect in peripheral microneme transport along the microtubules. Among the dynein heavy chains found in *T. gondii*, TGME49_294550 is present in the genome of all the apicomplexans (**Table S1**) and might be involved in this task, as this family is known to be involved in the long distance transport of vesicles and organelles [49].

Remarkably, DLC8a depletion also affected the apical positioning of the rhoptries, leading to a few mis-positioned organelles disseminated in the cytoplasm. Although some rhoptries were still apically positioned with their neck properly inserted into the conoid, organelle discharge and invasion were significantly impaired. The invasion phenotype might result from an

insufficient number of properly positioned rhoptries, given that the parasite is known to discharge rhoptries in uninfected-host cells prior to successful invasion [50]. Alternatively, the impairment in rhoptry discharge could result from a microneme exocytosis defect at the time of invasion, possibly due to the absence of MIC8, which was previously reported to be important for rhoptry discharge [51].

CEN2 is a marker for the lower boundary of the apical cap that is delineated by a ring of approximately six annuli. These peripheral annuli form a mysterious structure of unassigned function. The annuli have been described only in *T. gondii*, but are likely to be present in the coccidian subgroup of Apicomplexa. We report here a new marker of this structure, PAP2, which was identified by mass spectrometry during biotin-based proximity-labelling (BioID) of SAS6L and shown here to be associated with CEN2. It is found in most coccidians (**Dataset S1**). The previously described PAP1 protein [34] is conserved in some coccidian parasites (**Table S1**) and possesses a trichohyalin-like domain in addition to two coiled-coil domains. Trichohyalin is an intermediate filament-associated protein made of two EF-hand domains and a 28 aa-sequence repeat region [52] comparable to the one we observed in PAP1. Interestingly, a network of intermediate filament-like proteins, the alveolins, underlies the cytoplasmic face of the IMC and might interact with PAP1 [53]. Supporting this hypothesis, PAP1 has been found in the proteome of the subpellicular cytoskeleton of *T. gondii* [54] and the annuli are resistant to oryzalin-mediated microtubule depolymerization. Regarding PAP2, its sequence is predicted to include ARM repeats and a coiled-coil domain. Comparison of amino-acid sequences between PAP1 and PAP2 reveals no similarity. However, *in silico* protein modelling (Phyre2 server) suggests that both proteins share structural similarities with their central core forming a double stranded coiled-coil rod domain usually found in intermediate filament proteins.

Super-resolution microscopy revealed that peripheral annuli exhibit a complex and organized structure with distinct protein content. More precisely, CEN2-YFP appears as a dot surrounded by a ring of PAP1 and PAP2 proteins. In the absence of CEN2, we observed that PAP2 was lost and degraded. Currently, the peripheral annuli can only be observed by IFA, hence we cannot formally conclude that loss of annuli-associated proteins leads to the loss of the underlying structure. PAP1 and PAP2 are the only two specific markers of this structure and are predicted to be dispensable for tachyzoite survival [28]. Nevertheless, the PAP2 locus seems refractory to disruption despite several attempts using two different knockout strategies. The annuli have been hypothesized to participate in endocytosis or in dense granule secretion; however, no defect in dense granule secretion was observed in CEN2-depleted parasites or in PAP1-KO parasites (data not shown). The multiple roles of CEN2 and the concomitant disappearance of PAP2 from the annuli, together with the inability to obtain PAP2-KO parasites, hampers a functional assignment for these structures. In this context, we cannot formally conclude that the loss of CEN2 at the apical tip per se is responsible for the observed phenotype. Further investigation will be needed to unravel the contribution of these enigmatic structures.

In conclusion, we report the role of two conoidal protein, CEN2 and DLC8a, in microneme secretion that do not appear to play a role in conoid protrusion. However, the two proteins seem to act at different steps along the signalling cascade leading to microneme exocytosis. These findings support the current model that microneme secretion is dependent on Ca^{2+} pulses, while microtubules provide a track for the transport of these organelles to the conoid as suggested by the localization of DLC8a in extracellular protruded parasites. In addition, our study suggests a role for a microtubule-associated complex in rhoptry docking at the apical pole of the parasite. Importantly, both CEN2 and DLC8a might fulfill similar functions across the phylum as they do in *T. gondii*.

Materials and Methods

Molecular cloning

The sequence of the primers used for the cloning can be found in **Table S2**.

Myc-DLC8-iKD (inducible knock-down)

To generate the Tet-repressive knockdown of DLC8a, a PCR fragment encoding the TATi trans-activator, HXGPRT selection cassette, the TetO7S1 promoter and the c-Myc tag was generated using the KOD DNA polymerase (Novagen, Merk) with the vector 5'COR-pT8TATi1-HX-tetO7S1myc [55] as template and the primers DLC8a-7214/DLC8a-7215 that also carry 30 bp homology with the 5' end of DLC8a. To direct the insertion of the PCR product at the start of DLC8a locus, a specific sgRNA vector has been generated using the Q5 site-directed mutagenesis kit (New England Biolabs), the vector pSAG1::CAS9-GFPU6::sgUPRT as template [56] and the primer pair DLC8a-7378/gRNA-4883.

PAP1-3Ty-HXGPRT (Knock-in)

To generate the PAP1-3Ty-HXGPRT vector, a gDNA fragment corresponding to the C-terminus of PAP1 (TGGT1_242790A and B) was amplified by PCR using the primer pair PAP1_5505/PAP1_5506 and cloned into the *Kpn*I and *Nsi*I sites of the pTUB8-MIC13-3Ty-HX [57].

PAP2-3Ty-DHFR (Knock-in)

To generate the PAP2-3Ty-DHFR vector, a gDNA fragment of the C-terminal part of PAP2 (TGGT1_230340) was amplified by PCR using the primers PAP2_6308/PAP2_6309 and cloned into the *Apa*I and *Nsi*I sites of the Ct-ASP5-3Ty-DHFR [58].

PAP1-KO-DHFR (Knockout)

To generate the PAP1-KO, a PCR amplicon of the DHFR resistance cassette was generated using the KOD DNA polymerase (Novagen, Merk), the vector p2854-DHFR [59] as template and the primers PAP1_8995/PAP1_8996 that encode 30bp overhangs corresponding to the start and the 3' end of *PAP1*. A double CRISPR-Cas9 guide strategy was used to drive the insertion of the amplicon into the PAP1 locus. Two specific gRNAs were made as previously described. Then a PCR amplicon of one guide amplified using the primers 2nd-gRNA-F_6147/2nd-gRNA-R_6148 was sub-cloned into the other guide between the *KpnI* and *XhoI* restriction sites, thereby generating a dgRNA plasmid with two targeted sgRNAs.

Parasite culture and transfection

The *T. gondii* ΔKU80 RH strain was used throughout this study and tachyzoites were propagated in confluent Human Foreskin Fibroblasts (HFFs) with Dulbecco's modified Eagle's medium supplemented with 5% fetal bovine serum. Transfection of tachyzoites were performed as previously described [60] either with 15-20 μg of linearized plasmid for endogenous tagging or with a mix of 15ug Cas9-sgRNA plasmid and 10-20 μg of PCR product. Clonal populations were isolated by limited dilution and the presence of the recombinant locus was verified by PCR performed on genomic DNA with the primers outlined in Table S3, Figures S2 and S4 and the GoTaq polymerase (Promega). For the transient expression of eGFP-DLC8a, 100 μg of pmin-eGFP-DLC8a plasmid [31] was transfected into CEN2-iKD. Immediately after the electrical pulse, the transfected parasites were split into two dishes containing HFF either in the absence or in the presence of ATc. Extracellular parasites were collected 2 days post-transfection.

Immunofluorescence assay (IFA)

For IFA, parasite-infected HFF cells coated on coverslips were fixed with 4% paraformaldehyde (PFA)/0.05% glutaraldehyde (GA) in PBS for 10-12 min (for most of the antigen to be labelled) or with cold methanol for 8 min at -20°C (for α-Myc to detect MycDLC8a and for α-acetylated tubulin) and then processed with and without Triton X-100 respectively, as previously described [20]. Confocal and STED microscopy images were collected with a confocal laser scanning microscope LSM700 (Zeiss) and a TCS SP8 STED 3X microscope (Leica) respectively, at the Bioimaging Core Facility of the University of Geneva Medicine Faculty. For confocal data, the images were analysed using ImageJ and the z-stacks were projected using the maximum projection tool. For the STED microscopy, 3D reconstruction and projection were performed using Imaris 9.0 (Bitplane) and LasX (Leica) softwares respectively. Some images were contrast enhanced for figure presentation.

Western-blot

For immuno-blot analysis, pellets from extracellular tachyzoites were resuspended in PBS buffer, mixed with loading buffer under reducing condition (DTT), sonicated in a bioruptor (diagenode) and then boiled for 10 min before loading onto a SDS–PAGE gel. After running, wet-transfer was performed onto nitrocellulose membranes before probing with appropriate antibodies in 5% non-fat milk powder in PBS-0.05% Tween20. Bound secondary conjugated antibodies were visualized using the ECL system (for horseradish peroxidase) or detected directly (for the Alexa-Fluor-680-conjugated).

Plaque assay

Freshly egressed parasites were used to infect confluent HFF cells. These plates were incubated for 7 days ± ATc and then fixed with PFA/GA and stained with a crystal violet solution (Sigma).

Intracellular growth assay

Parasites pre-treated for 24h (ΔKU80 and CEN2-iKD) or 36h (ΔKU80 and DLC8a-iKD) ± ATc were allowed to grow on new confluent HFFs for 24h ± ATc before fixation with PFA/GA. IFA was then performed using anti-GAP45 antibodies and the number of parasites per vacuole was counted in 100 vacuoles from 3 independent experiments. The results are

presented as mean ± SD and the significance of the results has been assessed using an unpaired t-test.

Red/green invasion assay

Parasites pre-treated ± ATc for 48h (ΔKU80 and CEN2-iKD) or 60h (ΔKU80 and DLC8a-iKD) were used to perform the invasion assay as previously described [61]. The number of extracellular and intracellular parasites was determined by counting 100 parasites in duplicate for three independent experiments. Results are presented as mean ± SD and the significance of the results was assessed using an unpaired t-test.

Induced egress assay

Parasites were pre-treated for 18h (ΔKU80 and CEN2-iKD) or 30h (ΔKU80 and DLC8a-IKD) ± ATc. Freshly egressed parasites were then allowed to grow on new confluent HFFs for 30h ± ATc before adding either BIPPO (50 µM), A23187 from *Streptomyces chartreusensis* (3 µM) or DMSO for 8 min. IFAs were performed using α-GRA3 to stain the parasitophorous vacuole and α-GAP45 to stain the parasites. The average number of egressed vacuoles was determined by counting at least 100 vacuoles in duplicate for each condition and for three biological experiments. The results are presented as mean ± SD and the significance of the results has been assessed using an unpaired t-test.

Host cell attachment assay

Extracellular parasites expressing GFP and mutant cell lines were pre-treated ± ATc for 48h (ΔKU80 and CEN2-iKD) or 60h (ΔKU80 and DLC8a-iKD) and then mixed at a 50/50 ratio. The parasite mixture was added to HFF-coated coverslips ("assay") and centrifuged for 1 min at 1000 rpm, washed once and then fixed with PFA/GA for 10 min. In parallel, an aliquot of this mixture was stained with Hoechst for 20 min and fixed with PFA/GA for 10 min to determine the initial ratio on a Beckman Coulter Gallios flow cytometer ("control"). For the "assay", immunofluorescence (IFA) was performed using α-GAP45 antibodies to determine the ratio of attached parasites. The experiments have been performed in triplicates, 1000 parasites were counted by flow cytometry and 100 parasites by IFA. Percentage of GFP positive (internal control) and negative parasites (strain of interest) were calculated for both flow cytometry and microscopy methods. Efficiency of attachment was measured by calculating the ratio between the proportion of parasites attached to the host cell ("assay" %) and the proportion of parasite that were initially present in the mix ("control" %).

Microneme secretion assay

Freshly egressed parasites pre-treated ± ATc for 48h (ΔKU80 and CEN2-iKD) or 60h (ΔKU80 and DLC8a-iKD) were used to performed microneme secretion assay with 2% ethanol or 50 µM BIPPO as previously described [20]. Secretion was assessed by western-blot.

Rhoptry secretion assay

A phospho-STAT6 test was used to measure the ability of parasites to successfully secrete rhoptry proteins into the host cells. Briefly, freshly egressed DLC8-iKD parasites pre-treated ± ATc for 60 h were resuspended in cold DMEM at a concentration of 20.10^5 parasites/mL and 5.10^5 parasites were used to infect HFF coated coverslips. The plates were centrifuged 30 sec at 1100g to allow

parasites to attach and incubated for 20 min on ice to synchronize the invasion. Cells were then incubated at 37°C for 20 min and fixed with ice-cold methanol for 8 min at -20°C. Following blocking, immuno-detection was done using anti-PSTAT6 (Cell signaling 9361; 1/400) and the number of parasites associated to a PSTAT6 positive nucleus was determined. The experiments were done in triplicate and 100 parasites were counted each time.

Induced gliding assay

Motility was performed by video microscopy on a Nikon eclipse Ti inverted microscope at 37°C with either ΔKU80 and CEN2-iKD parasites pre-treated for 48h ± ATc or ΔKU80 and DLC8a-iKD parasites pre-treated for 60h ± ATc as previously described [62]. The type of gliding was evaluated in 100 parasites, in 3 biological replicates. The results are presented as mean ± SD and the significance of the results has been assessed using an unpaired t-test. Tracking of parasites was performed using the Manual Tracking plugin on ImageJ software.

Electron microscopy

For transmission electron microscopy, the *T. gondii* infected HFF cells were grown as monolayers on 13 mm round glass coverslips. After 78h treatment with ATc, cells were fixed with 2.5% glutaraldehyde (Electron Microscopy Sciences) and 2% paraformaldehyde (Electron Microscopy Sciences) in 0.1 M phosphate buffer (PB) at pH 7.4 for 1h at room temperature. Cells were then washed 5 ×5 min with 0.1 M sodium cacodylate buffer, pH 7.4 and post-fixed with 1% osmium tetroxide (Electron Microscopy Sciences) and 1.5% potassium ferrocyanide in 0.1 M sodium cacodylate buffer, pH 7.4 for 1h immediately followed by 1% osmium tetroxide (Electron Microscopy Sciences) in 0.1 M sodium cacodylate buffer pH 7.4 for 1h. Coverslips were then washed in double distilled water 2 × 5 min and *en block* stained with aqueous 1% uranyl acetate (Electron Microscopy Sciences) for 1h. After 5 min wash in double distilled water cells were dehydrated in graded ethanol series (2 × 50%, 70%, 90%, 95%, and 2 × absolute ethanol) for 3 min each wash. Dehydrated cells were infiltrated with Durcupan resin (Electron Microscopy Sciences) diluted with ethanol at 1:2, 1:1, 2:1 for 30 min each, and twice with pure Durcupan for 30 min each. Fresh Durcupan resin was added for additional 2h. Coverslip with grown cells faced down was placed on 1 mm-thick silicone ring filled with fresh resin which was placed on a glass slide coated with mold-separating agent (Gloorex). Finally, samples were polymerized at 65°C overnight in oven until resin was cured. The glass coverslip was removed from the resin disk by immersing alternately into hot water and liquid nitrogen.

Targeted parasitophorous vacuole inside HFF cells was marked on the resin surface using laser microdissection microscope (Leica Microsystems). Under stereo-microscope, marked area was cut out from the disk and glued with superglue to a blank resin block. Leica Ultracut UCT microtome (Leica Microsystems) and a glass knife were used to trim the cutting face. 70 nm ultrathin serial sections were cut with a diamond knife (DiATOME) and collected onto 2 mm single slot copper grids (Electron Microscopy Sciences) coated with Formvar plastic support film.

Sections were examined with Tecnai 20 TEM (FEI) operating at an acceleration voltage of 80 kV and images were collected by side-mounted MegaView III CCD

camera (Olympus Soft-Imaging Systems) controlled by iTEM acquisition software (Olympus Soft-Imaging Systems).

Focused Ion Beam Scanning Electron Microscopy (FIBSEM) and 3D Reconstruction

Sample for FIBSEM imaging were prepared as described above. Either whole resin block or large cut out area, containing the region of interest marked by laser microdissection microscope (Leica Microsystems) was glued onto a flat SEM stub with superglue and on each side of the block the silver conductive paste was applied. The mounted sample was gold coated with 20 nm thick layer of gold.

The imaged volume was acquired by FEI Helios NanoLab G3 UC DualBeam microscope (FEI). Ion beam was used in conjunction with a gas injection system to deposit a thick (~1.5 µm) layer of platinum on the top surface of the sample above the region of interest to reduce the FIB milling artefacts. The imaging surface was exposed by creating the front trench and subsequently two side trenches were created using 21 nA of focused ion beam current at 30 kV voltage.

AutoSlice and View G3 software (FEI) was used to acquire the serial SEM images. Focused ion beam at current of 2.5 pA and 30kV of acceleration voltage was applied to mill 10 nm layer from imaging face and freshly exposed surface was imaged with back scattered electron beam current of 400 pA at acceleration voltage of 2 kV, the dwell time of 9 µsec/pixel and at the resolution of 4 nm/pixel. The size of the final imaged volume in *x*-, *y*- and *z*-dimension was 5751 × 1503 × 810 pixels corresponding to 23 × 6 × 8.1 µm for DLC8a-iKD (+78h ATc). The final volume of cropped parasitophorous vacuole was 10.99 × 6 × 8.1 µm.

Serial images were combined into single image stacks and aligned using the FIJI program (fiji.sc/). After alignment, images were scaled down to have volume with isotropic voxel properties of the 10 nm/pixel in all *x*-, *y*-, and *z*-dimension.

3D reconstruction was generated by semi-automated approach using Ilastik software (ilastik.org) and 3D model was visualized using the Blender program (v.2.79; blender.org).

Antibody list

Primary antibodies used in this study: monoclonal mouse α-Ty (hybridoma BB2, 1:10 IFA, 1:10 WB or ascyte 1:1000 IFA [63]), α-Myc (hybridoma mAb 9E10, 1:10 IFA, 1:10 WB), α-GFP (Roche, 1:1000 WB), α-actin (hybridoma, 1:10 IFA, 1:10 WB [64], α-MIC2 (hybridoma, generous gift from Dr V. carruthers, 1:10 IFA, 1:10 WB), α-ISP1 (1:1000 IFA [65], a generous gift from Dr P. Bradley), α-GRA1 (1:3000 WB, Anawa), α-ROP7 T4-3H1, α-RON9 (hybridomas, generous gift from Dr J-F. Dubremetz, 1:10 IFA, 1:10 WB) and polyclonal rabbit α-catalase (1:2000, [66]), α-CEN1 (1:1000 IFA, kerafast), α-ARO (1:1000 IFA, [15]) , α-GAP45 (1:10.000 IFA, [67]), α-IMC1 (1:1000 IFA, [61]), α-MIC6 (1:1000 WB, [68]), and α-PSTAT6 (1:400 IFA, Cell signaling 9361). Secondary antibodies used in this study: anti-mouse and anti-rabbit HRP (Sigma), Alexa-Fluor-680-conjugated goat anti-rabbit and anti-mouse IgG antibodies, Alexa-Fluor-488-conjugated goat anti-rabbit and anti-mouse IgG antibodies and Alexa-Fluor-594-conjugated goat anti-rabbit and anti-mouse IgG antibodies (Thermofisher).

Acknowledgements

This research was supported by Swiss National Science Foundation (FN3100A0-116722 to DSF) and by Scientific & Technological Cooperation Programme Switzerland - Rio de Janeiro (STCPSRJ) to K.F (IZRJZ3_164183). Results incorporated in study received funding from the European Research Council (ERC) under the European Union's Horizon 2020 research and innovation programme under Grant agreement no. 695596. Authors would like to thank Carmen T. Gómez de León for the cloning of PAP1, Dr. Ke Hu for the plasmid pmin-eGFP-DLC8a, Dr. Sébastien Besteiro for sharing the oryzalin, Dr. Damien Jacot as well as the Proteomics Core Facility, Faculty of Medicine of Geneva for the mass spectrometry analysis leading to the identification of PAP2 protein at the peripheral annuli, Dr. Iryna Nikonenko from the EM facility at the Faculty of Medicine of Geneva (PFMU) for her expertise and help with Helios FIBSEM image acquisition, Dr. François Prodon from the Bioimaging Core Facility of the Faculty of Medicine of Geneva for his technical assistance with the STED and Phyre2 web portal for *in silico* protein modelling. We also thank Dr. Maryse Lebrun for the LIC-CEN2-YFP construct, Dr. David Sibley for the CRISPR-Cas9 vector. We are grateful to Aarti Krishnan and Joseph Curran for their critical reading of the manuscript.

Author contributions

D.S-F, K.F and G.L conceived the project. K.F, G.L D.J.D and B.M. designed, performed and interpreted the experimental work. D.S-F and K.F supervised the research. G.L, D.J.D, K.F and D.S.-F wrote the paper.

Conflict of Interest Statement

The authors declare no conflict of interest.

References

1. Goodson H V, Jonasson EM. Microtubules and Microtubule-Associated Proteins. *Cold Spring Harb Perspect Biol*. 2018.
2. Brooks CF, Francia ME, Gissot M, Croken MM, Kim K, Striepen B. *Toxoplasma gondii* sequesters centromeres to a specific nuclear region throughout the cell cycle. *PNAS*. 2011;108(9). doi:10.1073/pnas.1006741108
3. Jacot D, Daher W, Soldati-favre D. *Toxoplasma gondii* myosin F , an essential motor for centrosomes positioning and apicoplast inheritance. *EMBO J*. 2013;32(12):1702-1716. doi:10.1038/emboj.2013.113
4. Chen C, Gubbels M. The *Toxoplasma gondii* centrosome is the platform for internal daughter budding as revealed by a Nek1 kinase mutant. *J Cell Sci*. 2013:3344-3355. doi:10.1242/jcs.123364
5. Morlon-Guyot J, Berry L, Chen C-T, Gubbels M-J, Lebrun M, Daher W. The *Toxoplasma gondii* Calcium Dependent Protein Kinase 7 is involved in early steps of parasite division and is crucial for parasite survival. *Cell Microbiol*. 2014;16(1):95-114. doi:10.1111/cmi.12186.The
6. Anderson-White B, Beck JR, Chen C, Meissner M, Peter J, Gubbels M. Cytoskeleton assembly in *Toxoplasma gondii* cell division. *Int Rev Cell Mol Biol*. 2014:1-31. doi:10.1016/B978-0-12-394309-

5.00001-8.Cytoskeleton
7. Hu K, Roos DS, Murray JM. A novel polymer of tubulin forms the conoid of *Toxoplasma gondii*. *J Cell Biol*. 2002;156(6):1039-1050. doi:10.1083/jcb.200112086
8. González D, Mondragón M, González S, Mondragón R. Induction and regulation of conoid extrusion in *Toxoplasma gondii*. *Cell Microbiol*. 2009;11(March):967-982. doi:10.1111/j.1462-5822.2009.01304.x
9. Carruthers VB, Tomley FM. Receptor-ligand interaction and invasion: Microneme proteins in apicomplexans. *Subcell Biochem*. 2008;47:33-45. doi:10.1111/jiec.12759
10. Lamarque M, Besteiro S, Papoin J, et al. The RON2-AMA1 Interaction is a Critical Step in Moving Junction-Dependent Invasion by Apicomplexan Parasites. *PLoS Pathog*. 2011;7(2). doi:10.1371/journal.ppat.1001276
11. Kats LM, Cooke BM, Coppel RL, Black CG. Protein Trafficking to Apical Organelles of Malaria Parasites – Building an Invasion Machine. *Traffic*. 2008:176-186. doi:10.1111/j.1600-0854.2007.00681.x
12. Leung JM, He Y, Zhang F, et al. Stability and function of a putative microtubule-organizing center in the human parasite *Toxoplasma gondii*. *Mol Biol Cell*. 2017;28(10):1361-1378. doi:10.1091/mbc.e17-01-0045
13. Paredes-santos TC, Souza W De, Attias M. Dynamics and 3D organization of secretory organelles of *Toxoplasma gondii*. *J Struct Biol*. 2012;177(2):420-430. doi:10.1016/j.jsb.2011.11.028
14. Dubremetz JF. Rhoptries are major players in *Toxoplasma gondii* invasion and host cell interaction. *Cell Microbiol*. 2007;9:841-848. doi:10.1111/j.1462-5822.2007.00909.x
15. Mueller C, Klages N, Jacot D, et al. The *toxoplasma* protein ARO mediates the apical positioning of rhoptry organelles, a prerequisite for host cell invasion. *Cell Host Microbe*. 2013;13(3):289-301. doi:10.1016/j.chom.2013.02.001
16. Mueller C, Samoo A, Hammoudi P, Klages N, Kallio JP. Structural and functional dissection of *Toxoplasma gondii* armadillo repeats only protein. *J Cell Sci*. 2016;129:1031-1045. doi:10.1242/jcs.177386
17. Frénal K, Tay CL, Bushell ES, et al. Global Analysis of Apicomplexan Protein S-Acyl Transferases Reveals an Enzyme Essential for Invasion. *Traffic*. 2013:895-911. doi:10.1111/tra.12081
18. Beck JR, Fung C, Straub KW, et al. A Toxoplasma Palmitoyl Acyl Transferase and the Palmitoylated Armadillo Repeat Protein TgARO Govern Apical Rhoptry Tethering and Reveal a Critical Role for the Rhoptries in Host Cell Invasion but Not Egress. *PLoS Pathog*. 2013;9(2). doi:10.1371/journal.ppat.1003162
19. Graindorge A, Frénal K, Jacot D, Salamun J. The Conoid Associated Motor MyoH Is Indispensable for *Toxoplasma gondii* Entry and Exit from Host Cells. *PLoS Pathog*. 2016:1-26. doi:10.1371/journal.ppat.1005388
20. Bullen HE, Jia Y, Carruthers V, et al. Phosphatidic Acid-Mediated

Signaling Regulates Microneme Secretion in *Toxoplasma* Article Phosphatidic Acid-Mediated Signaling Regulates Microneme Secretion in Toxoplasma. *Cell Host Microbe*. 2016:349-360. doi:10.1016/j.chom.2016.02.006

21. Darvill N, Dubois DJ, Rouse SL, et al. Structural Basis of Phosphatidic Acid Sensing by APH in Apicomplexan Parasites. *Structure*. 2018;26(8):1059-1071.e6. doi:10.1016/j.str.2018.05.001
22. Dubois DJ, Soldati-Favre D. Biogenesis and secretion of micronemes in *Toxoplasma gondii* . *Cell Microbiol*. 2019;(February):e13018. doi:10.1111/cmi.13018
23. Farrell A, Thirugnanam S, Lorestani A, et al. A DOC2 Protein Identified by Mutational Profiling is Essential for Apicomplexan Parasite Exocytosis. *Science (80-)*. 2012;335(6065):218-221. doi:10.1126/science.1210829.A
24. Coleman BI, Saha S, Sato S, et al. A Member of the Ferlin Calcium Sensor Family Is Essential for *Toxoplasma gondii* Rhoptry Secretion. *MBio*. 2018;9(5):1-14.
25. Long S, Anthony B, Drewry LL, Sibley LD. A conserved ankyrin repeat-containing protein regulates conoid stability, motility and cell invasion in *Toxoplasma gondii*. *Nat Commun*. 2017;8(1). doi:10.1038/s41467-017-02341-2
26. Nagayasu E, Hwang Y-C, Liu J, Murray JM, Hu K. Loss of a doublecortin (DCX)-domain protein causes structural defects in a tubulin-based organelle of *Toxoplasma gondii* and impairs host-cell invasion. *Mol Biol Cell*. 2017;28(3):411-428. doi:10.1091/mbc.e16-08-0587
27. Katris NJ, van Dooren GG, McMillan PJ, Hanssen E, Tilley L, Waller RF. The Apical Complex Provides a Regulated Gateway for Secretion of Invasion Factors in *Toxoplasma*. *PLoS Pathog*. 2014;10(4). doi:10.1371/journal.ppat.1004074
28. Sidik SM, Huet D, Ganesan SM, et al. A Genome-Wide CRISPR Screen in *Toxoplasma* Identifies Essential Apicomplexan Genes. *Cell*. 2016;166(6):29-39. doi:10.1016/j.artmed.2015.09.007.Information
29. Selvapandiyan A, Kumar P, Morris JC, Salisbury JL, Wang CC, Nakhasi HL. Centrin1 Is Required for Organelle Segregation and Cytokinesis in *Trypanosoma brucei*. *Mol Biol Cell*. 2007;18(September):3290-3301. doi:10.1091/mbc.E07
30. Selvapandiyan A, Kumar P, Salisbury JL, Wang CC, Nakhasi HL. Role of Centrins 2 and 3 in Organelle Segregation and Cytokinesis in *Trypanosoma brucei*. *PLoS One*. 2012;7(9):1-11. doi:10.1371/journal.pone.0045288
31. Hu K, Johnson J, Florens L, et al. Cytoskeletal components of an invasion machine - The apical complex of *Toxoplasma gondii*. *PLoS Pathog*. 2006;2(2):0121-0138. doi:10.1371/journal.ppat.0020013
32. de Leon JC, Scheumann N, Beatty W, et al. A sas-6-like protein suggests that the *Toxoplasma* conoid complex evolved from flagellar components. *Eukaryot Cell*.

2013;12(7):1009-1019. doi:10.1128/EC.00096-13

33. Sanders M., Salisbury J. Centrin-mediated Microtubule Severing during Flagellar Excision in *Chlamydomonas reinhardtii*. *J Cell Biol*. 1989;108(May):1751-1760.
34. Suvorova ES, Francia M, Striepen B, White MW. A Novel Bipartite Centrosome Coordinates the Apicomplexan Cell Cycle. *PLoS Biol*. 2015;13(3):1-29. doi:10.1371/journal.pbio.1002093
35. Frénal K, Jacot D, Hammoudi PM, Graindorge A, MacO B, Soldati-Favre D. Myosin-dependent cell-cell communication controls synchronicity of division in acute and chronic stages of *Toxoplasma gondii*. *Nat Commun*. 2017;8. doi:10.1038/ncomms15710
36. Reck-Peterson SL, Redwine WB, Vale RD, Carter AP. The cytoplasmic dynein transport machinery and its many cargoes. *Nat Rev Mol Cell Biol*. 2018;19(June). doi:10.1038/s41580-018-0004-3
37. Wickstead B, Gull K. Dyneins Across Eukaryotes : A Comparative Genomic Analysis. *Traff*. 2007:1708-1721. doi:10.1111/j.1600-0854.2007.00646.x
38. Qureshi BM, Hofmann NE, Arroyo-Olarte RD, et al. Dynein light chain 8a of *Toxoplasma gondii*, a unique conoid-localized ß-strand-swapped homodimer, is required for an efficient parasite growth. *FASEB J*. 2013;27(3):1034-1047. doi:10.1096/fj.11-180992
39. Lentini G, Kong-hap M, Hajj H El, et al. Identification and characterization of *Toxoplasma* SIP , a conserved apicomplexan cytoskeleton protein involved in maintaining the shape , motility and virulence of the parasite. *Cell Microbiol*. 2015;17(August 2014):62-78. doi:10.1111/cmi.12337
40. Morrissette NS, Sibley LD. Disruption of microtubules uncouples budding and nuclear division in *Toxoplasma gondii*. *J Cell Sci*. 2002;115(Pt 5):1017-1025.
41. Howard BL, Harvey KL, Stewart RJ, et al. Identification of Potent Phosphodiesterase Inhibitors that Demonstrate Cyclic Nucleotide-Dependent Functions in Apicomplexan Parasites. *ACS Chem Biol*. 2015;10:1145-1154. doi:10.1021/cb501004q
42. Ong YC, Reese ML, Boothroyd JC. *Toxoplasma* Rhoptry Protein 16 (ROP16) subverts host function by direct tyrosine phosphorylation of STAT6. *J Biol Chem*. 2010;285(37):28731-28740. doi:10.1074/jbc.M110.112359
43. Nishi M, Hu K, Murray JM, Roos DS. Organellar dynamics during the cell cycle of *Toxoplasma gondii*. *J Cell Sci*. 2008;121(Pt 9):1559-1568. doi:10.1242/jcs.021089
44. Ouologuem DT, Roos DS. Dynamics of the *Toxoplasma gondii* inner membrane complex. *J Cell Sci*. 2014:3320-3330. doi:10.1242/jcs.147736
45. Bullen HE, Soldati-favre D. A central role for phosphatidic acid as a lipid mediator of regulated exocytosis in apicomplexa. *FEBS Lett*. 2016;590:2469-2481. doi:10.1002/1873-3468.12296
46. Sehring IM, Klotz C, Beisson J, Plattner H. Rapid downregulation of

the Ca2+-signal after exocytosis stimulation in *Paramecium* cells: Essential role of a centrin-rich filamentous cortical network, the infraciliary lattice. *Cell Calcium*. 2009;45(1):89-97. doi:10.1016/j.ceca.2008.06.004

47. Trojan P, Krauss N, Choe HW, Gießl A, Pulvermüller A, Wolfrum U. Centrins in retinal photoreceptor cells: Regulators in the connecting cilium. *Prog Retin Eye Res*. 2008;27(3):237-259. doi:10.1016/j.preteyeres.2008.01.003
48. Kremer K, Kamin D, Rittweger E, et al. An Overexpression Screen of *Toxoplasma gondii* Rab- GTPases Reveals Distinct Transport Routes to the Micronemes. *PLoS Pathog*. 2013;9(3). doi:10.1371/journal.ppat.1003213
49. Kardon JR, Vale RD. Regulators of cytoplasmic Dynein motor. *Nat Rev Mol Cell Biol*. 2009;10(12):854-865. doi:10.1038/nrm2804.DATABASES
50. Koshy AA, Dietrich HK, Christian DA, et al. *Toxoplasma* co-opts host cells it does not invade. *PLoS Pathog*. 2012;8(7):18. doi:10.1371/journal.ppat.1002825
51. Kessler H, Herm-Gotz A, Hegge S, et al. Microneme protein 8 - a new essential invasion factor in *Toxoplasma gondii*. *J Cell Sci*. 2008;121(7):947-956. doi:10.1242/jcs.022350
52. Fietz MJ, McLaughlan CJ, Campbell MT, Rogers GE. Analysis of the sheep trichohyalin gene: Potential structural and calcium- binding roles of trichohyalin in the hair follicle. *J Cell Biol*. 1993;121(4):855-865. doi:10.1083/jcb.121.4.855
53. Gould SB, Tham WH, Cowman AF, McFadden GI, Waller RF. Alveolins, a new family of cortical proteins that define the protist infrakingdom Alveolata. *Mol Biol Evol*. 2008;25(6):1219-1230. doi:10.1093/molbev/msn070
54. Gómez de León CT, Díaz Martín RD, Mendoza Hernández G, González Pozos S, Ambrosio JR, Mondragón Flores R. Proteomic characterization of the subpellicular cytoskeleton of *Toxoplasma gondii* tachyzoites. *J Proteomics*. 2014;111:86-99. doi:10.1016/j.jprot.2014.03.008
55. Salamun J, Kallio JP, Daher W, Soldati-favre D, Kursula I. Structure of *Toxoplasma gondii* coronin , an actin-binding protein that relocalizes to the posterior pole of invasive parasites and contributes to invasion and egress. *FASEB J*. 2014;(28):4729–4747. doi:10.1096/fj.14-252569
56. Shen B, Brown KM, Lee TD, Sibley LD. Efficient Gene Disruption in Diverse Strains of *Toxoplasma gondii* Using CRISPR / CAS9. *MBio*. 2014;5(3):1-11. doi:10.1128/mBio.01114-14.Editor
57. Sheiner L, Santos JM, Klages N, et al. *Toxoplasma gondii* transmembrane microneme proteins and their modular design. 2010;77(4):912-929.
58. Hammoudi PM, Jacot D, Mueller C, et al. Fundamental Roles of the Golgi-Associated *Toxoplasma* Aspartyl Protease, ASP5, at the Host-Parasite Interface. *PLoS Pathog*. 2015;11(10):1-32. doi:10.1371/journal.ppat.1005211
59. Donald RGK, David S. Stable

molecular transformation of *Toxoplasma gondii* : A selectable dihydrofolate reductase-thymidylate synthase marker based on drug-resistance mutations in malaria. 1993;90(December):11703-11707.
60. Soldati D, Boothroyd JC. Transient transfection and expression in the obligate intracellular parasite *Toxoplasma gondii*. *Science (80-).* 1993;260(5106):349-352.
61. Frénal K, Marq JB, Jacot D, Polonais V, Soldati-Favre D. Plasticity between MyoC- and MyoA-glideosomes: an example of functional compensation in *Toxoplasma gondii* invasion. *PLoS Pathog*. 2014;10(10):e1004504. doi:10.1371/journal.ppat.1004504
62. Hammoudi P, Maco B, Soldati-favre D. *Toxoplasma gondii* TFP1 is an essential transporter family protein critical for microneme maturation and exocytosis. *Mol Microbiol*. 2018;109:225-244. doi:10.1111/mmi.13981
63. Bastin P, Bagherzadeh A, Matthews KR, Gull K. A novel epitope tag system to study protein targeting and organelle biogenesis in *Trypanosoma brucei*. *Mol Biochem Parasitol*. 1996;77.
64. Herm-gotz A, Weiss S, Stratmann R, et al. *Toxoplasma gondii* myosin A and its light chain : a fast , single-headed , plus-end-directed motor. *EMBO J*. 2002;21(9):2149-2158.
65. Beck JR, Rodriguez-fernandez IA, Leon JC De, et al. A Novel Family of *Toxoplasma* IMC Proteins Displays a Hierarchical Organization and Functions in Coordinating Parasite Division. *PLoS Pathog*. 2010;6(9). doi:10.1371/journal.ppat.1001094
66. Ding M, Clayton C, Soldati D, Biologie M, Feld IN. *Toxoplasma gondii* catalase : are there peroxisomes in *Toxoplasma* ? *J Cell Sci*. 2000;2419:2409-2419.
67. Frenal K, Polonais V, Marq J, Stratmann R, Limenitakis J. Article Functional Dissection of the Apicomplexan Glideosome Molecular Architecture. *Cell Host Microbe*. 2010:343-357. doi:10.1016/j.chom.2010.09.002
68. Meissner M, Schlu D, Soldati D. Role of *Toxoplasma gondii* Myosin A in Powering Parasite Gliding and Host Cell Invasion. *Sci Rep*. 2002;298(October):837-841.

Figure legends

Figure 1. CEN2 is essential for the tachyzoite lytic cycle

A. Immunofluorescence time-course of the down-regulation of CEN2-YFP upon ATc treatment. IMC1 stains the periphery of the parasites. The white arrows point to the centrosomes while the yellow arrowheads point to the enlarged basal pole of the parasites. Scale bars: 2 μm. B. Scheme of the 48h lytic cycle of tachyzoite. Freshly egressed parasites are able to glide and attach to an uninfected host cell before reorientation and invasion. Multiple rounds of division occur within the parasitophorous vacuole (PV) before the parasites egress, lyse the cell and re-infect the neighbouring uninfected cells. C. Plaque assay performed over 7 days with the parental (ΔKU80) and the CEN2 inducible (CEN2-iKD) strains in the presence or absence of ATc. CEN2-iKD parasites show a strong defect in their lytic cycle. Scale bars: 0.5 cm. C. Intracellular growth assay performed after 0, 48 and 72h of ATc treatment. No defect was detected for the CEN2-depleted parasites.

Figure 2. CEN2 is critical for microneme secretion

A. Invasion assay performed after 48h ± ATc on the parental (ΔKU80) and the CEN2 inducible strains (CEN2-iKD) revealing a severe defect in the invasion efficiency of the CEN2-depleted parasites. B. Egress assay performed after 48h ± ATc using BIPPO as inducer. The CEN2-depleted parasites exhibit a strong defect in their capacity to egress from the host cell. C. Motility assay performed after 48h ± ATc using BIPPO as inducer. The different types of gliding motility have been quantified by video-microscopy (see Figure S1B and C). D. Western blot analysis of microneme protein MIC2 secretion after induction with 2% ethanol for 30 min. The dense granule protein 1 (GRA1) shows the constitutive secretion of dense granules and catalase (CAT) shows the integrity of the parasites. ESA: excreted secreted antigens, pMIC2: processed MIC2. E. Attachment assay performed after 48h ± ATc. The attachment efficiency of the CEN2-depleted parasites is strongly affected. For A, B, C and E, results are presented as mean ± SD. The significance of the results has been assessed using an unpaired t-test. The two-tailed P-values are written on the graphs. F. The localization and integrity of the apical secretory organelles were checked after 0 and 48h of ATc treatment using the markers MIC2, which stains the micronemes and ARO, anchored at the surface of the rhoptries. GAP45 stains the periphery of the parasites and actin (ACT1) shows the cytosol. The integrity of the apical cap of the IMC was verified using the marker ISP1. Scale bars: 2 μm.

Figure 3. CEN2, PAP1 and PAP2 colocalize to the annuli and form a complex structure

A. Stimulated emission depletion (STED) microscopy 3D projection of intracellular tachyzoites of *T. gondii* expressing CEN2-YFP/PAP1-3Ty. PAP1-3Ty staining is visualized using an anti-Ty antibody (red). x Scale bar: 1 μm. A scheme depicts the parasite organization in the imaged vacuole P1 and P2 = parasite 1 and parasite 2. B. 3D STED surface reconstruction of the apical part of parasite 1 (P1) showing that CEN2-YFP staining is surrounded by PAP1-3Ty staining. Scale bar: 0.4 μm. C. IFA of CEN2-YFP in wild type and PAP1-KO parasites. GAP45 stains the periphery of the parasites. Scale bar: 2 μm. In the absence of PAP1, CEN2 still localizes to

the annuli (C) and is not destabilized as demonstrated by western blot using anti-GFP antibodies and catalase (CAT) as a loading control (D). E. Plaque assay performed over 7 days with the CEN2-YFP-iKD and CEN2-YFP-iKD/PAP1-KO strains in presence or absence of ATc. No deleterious effect on the tachyzoite lytic cycle was monitored upon PAP1 deletion. F. STED microscopy 3D projection of intracellular tachyzoites expressing CEN2-YFP/PAP2-3Ty. PAP2-3Ty staining is visualized using an anti-Ty antibody (red). Scale bar: 1 μm. A scheme depicts the parasite organization in the imaged vacuole. P1-4 = parasite 1-4. G. 3D STED surface reconstruction of the apical part of parasite 3 (P3) and parasite 4 (P4) showing the CEN2-YFP surrounded by PAP2-3Ty. Scale bar: 0.4 μm.

Figure 4. CEN2 is critical for the architecture of the peripheral annuli

A. ΔKU80 (control), CEN2-YFP-iKD, PAP1-3Ty and PAP2-3Ty parasites have been treated with DMSO or 0.5nM oryzalin. Oryzalin treatment disturbs the cortical microtubules as shown in the control but not the apical localization of CEN2, PAP1 or PAP2. GAP45 stains the periphery of the parasites. Scale bars: 2 μm. B. Immunofluorescence performed on intracellular CEN2-iKD parasites stably expressing the endogenously tagged peripheral annuli protein 2 (PAP2). Upon ATc treatment, PAP2 staining is affected in its intensity and localization but is not homogenous within a vacuole. The number of vacuoles exhibiting a normal PAP2 staining has been quantified and is strongly decreased in CEN2-depleted parasites. Results are presented as mean ± SD and their significance has been assessed using an unpaired t-test. The two-tailed P-values are written on the graph. C. The expression and stability of PAP2 has been assessed by western-blot using the anti-Ty antibodies to detect the endogenously tagged protein and anti-catalase (CAT) as a loading control.

Figure 5. DLC8a localizes upstream of the secretory organelles and is critical for tachyzoite lytic cycle

A. IFA performed on intracellular parasite expressing the inducible N-terminally tagged DLC8a (MycDLC8a). MycDLC8a is found at the apical pole of the parasites as well as at the centrosome where it partially co-localizes with CEN1 and CEN2. Co-staining of MycDLC8a with markers of the micronemes (MIC6) and rhoptries (ARO) revealed that MycDLC8a localization is upstream of these secretory organelles. IFAs with CEN1 and MIC6 have been fixed with cold methanol while IFAs with CEN2 and ARO have been fixed with PFA/GA. Scale bars: 2 μm. B. In extracellular parasites, MycDLC8a staining is found at the apical end of the conoid in non-stimulated conditions and covering the conoid in protruded conditions (+A23187). IMC1 stains the periphery of the parasite. Scale bars: 1 μm. C. Immunofluorescence of Myc-DLC8a-iKD parasites treated either with DMSO or 0.5nM oryzalin for 24hours showing that DLC8a remains apical during cortical microtubule depolymerization. Scale bars: 2 μm. D-E. The regulation of MycDLC8a-iKD was assessed by IFA after 48h ± ATc (D) and by western blot (E) using anti-Myc antibodies. MycDLC8a reached undetectable levels after 48h of ATc treatment. Scale bars: 2 μm. F. Plaque assay performed over 7 days with the parental (ΔKU80) and the MycDLC8a inducible (MycDLC8a-iKD) strains in the presence or absence of ATc. MycDLC8a-iKD parasites do not form plaques in the

presence of ATc confirming a strong growth defect. Scale bars: 0.5 cm. G. Intracellular growth assay performed with ΔKU80 and MycDLC8a-iKD after a 60h pre-treatment ± ATc. No significant defect was noticed between the parental and the mutant strains. Results are presented as mean ± SD

Figure 6. DLC8a is critical for microneme secretion

A. Red/green invasion assays performed with freshly egressed ΔKU80 and MycDLC8a-iKD parasites after a 60h pre-treatment ± ATc. DLC8a depleted parasites are severely impacted in their invasion capacity. B. Microneme secretion assay carried out with freshly egressed ΔKU80 and MycDLC8a-iKD parasites pre-treated for 60h ± ATc and analysed by western blot. Neither ethanol nor BIPPO induce MIC2 secretion in DLC8a depleted parasites. GRA1 attests to the constitutive secretion of dense granules. ESA: excreted secreted antigens, pMIC2: processed MIC2. C. IFA performed on intracellular parasites treated ± ATc for 60h to assess the integrity and positioning of the micronemes. No defect was observed for the two proteins MIC2 and MIC6. Scale bars: 2 μm. D. Attachment assay performed with freshly egressed ΔKU80 and MycDLC8a-iKD parasites pre-treated for 60h ± ATc. A drop in the attachment efficiency of the parasites depleted in MycDLC8a can be observed. E. Induced egress assay performed on parasites treated for 60h ± ATc. Egress was induced with either the calcium ionophore A23187 or with BIPPO. A modest defect in egress was observed in the BIPPO-stimulated condition. F. Gliding assay performed by video-microscopy on parasites pre-treated for 60h ± ATc. No defect in motility was recorded. For A, D, E and F, results are presented as mean ± SD. The significance of the results has been assessed using an unpaired t-test and the two-tailed P-values are written on the graphs.

Figure 7. Mature rhoptries are found dispersed in the cytoplasm upon DLC8a depletion

A. IFA on intracellular parasites treated ± ATc for 60h to assess the integrity and positioning of the rhoptries. In MycDLC8a depleted parasites, the staining of the rhoptry surface protein ARO appears elongated, the staining of the rhoptry neck protein RON9 appears more punctate as well as the pattern of rhoptry bulb protein ROP7. Scale bars: 2 μm. B-D. A parasitophorous vacuole of the MycDLC8a-iKD cell line treated for 78 h with ATc was imaged by FIBSEM. Selected slices throughout the imaged volume are presented and show tachyzoites with disperse rhoptrie localizations (yellow r). C and D are images 590 nm and 750 nm deeper relative to image B. c: conoid, d: dense granules, m: mitochondrion, n: nucleus, r: rhoptry, tvn: tubulovesicular network; scale bars: 1 μm. E. 3D model of the tachyzoite highlighted with asterisk in B-D. Tachyzoite plasma membrane is in cyan, conoid in black, nucleus in light blue and rhoptries in orange. F-G. The ability of the ΔKU80 and MycDLC8a-iKD parasites to secrete their rhoptries was assessed using a Phospho-STAT6 test. It revealed a significant defect in the ROP16 secretion for the MycDLC8a depleted parasites. ARO-iKD parasites were used as a control since they present dispersed rhoptries under ATc treatment. F. Left panel: representative IFA of HFF monolayers infected with ATc-treated parasites. Parasites were stained

with an anti-ACT1 (actin) antibody, host cell nuclei were stained with DAPI and cells in which rhoptry have been discharged are stained with an anti-STAT6-P antibody. Right panel: graph representing the percentage of STAT6 positive nuclei associated with a parasite. Results are presented as mean ± SD. The significance of the results has been assessed using an unpaired t-test and the two-tailed P-values are written on the graph.

Figure 8. CEN2 and DLC8a are two independent actors of organelle exocytosis

A. IFA on intracellular parasites MycDLC8a-iKD expressing CEN2-YFP showing that depletion of DLC8a with ATc does not affect CEN2-YFP labelling. Scale bars: 2 μm. B. Western blot analysis of CEN2-YFP level (using anti-GFP antibodies) in CEN2-YFP/MycDLC8a-iKD parasites in untreated or ATc-treated parasites. Catalase (CAT) is used as a loading control. C. Western blot analysis of eGFP-DLC8a level in either ΔKU80 or CEN2-iKD parasites transiently transfected with eGFP-DLC8a and treated ± ATc for 48h. The level of eGFP-DLC8a remains the same even when CEN2-YFP is downregulated by the addition of ATc.

Figure 1

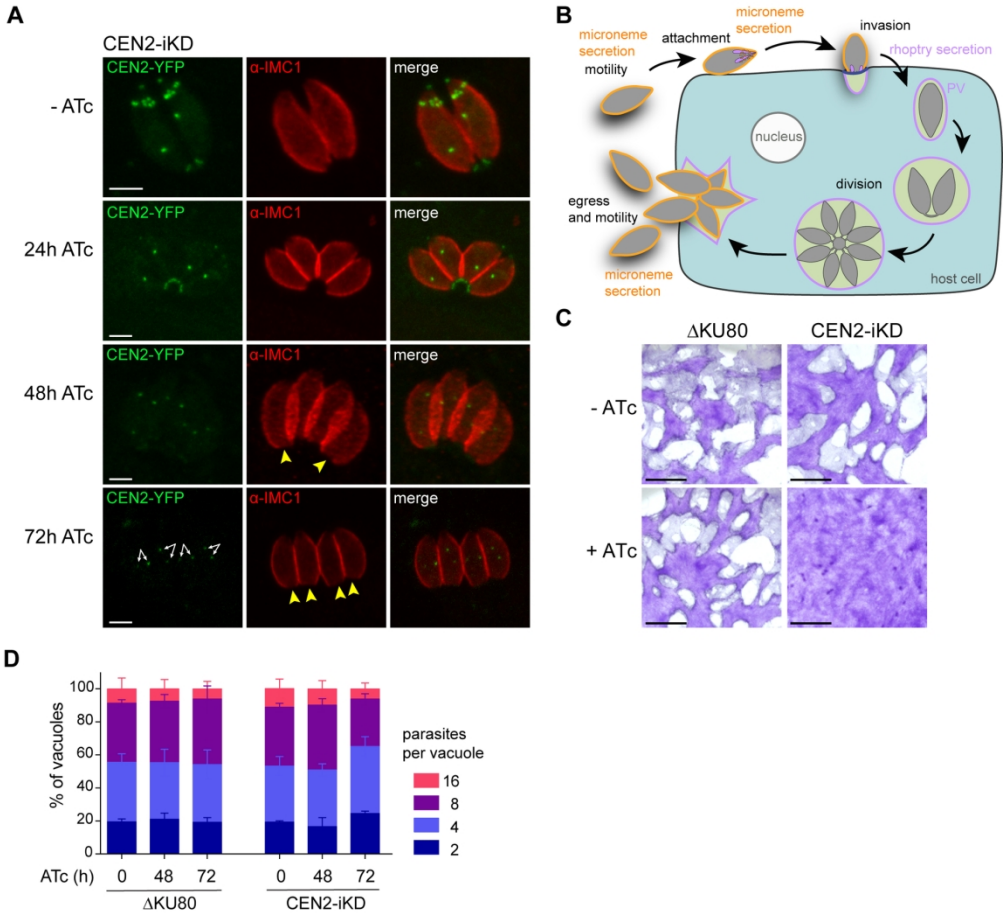

Figure 1

165x156mm (300 x 300 DPI)

Figure 2

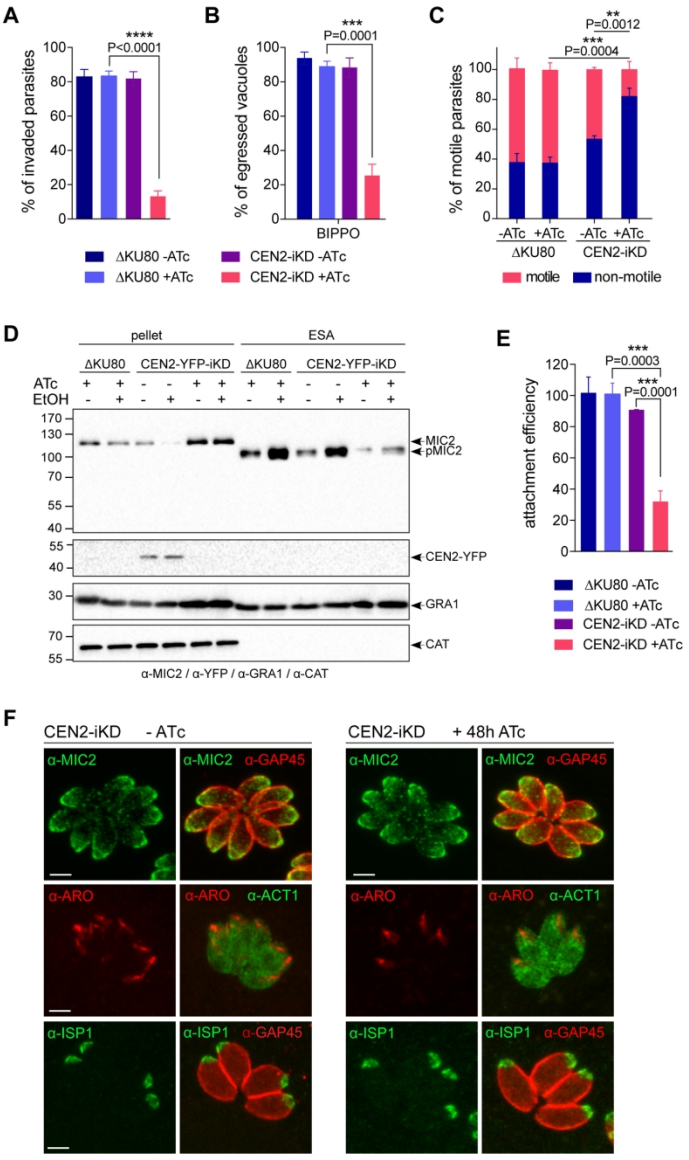

Figure 2

125x220mm (300 x 300 DPI)

Figure 3

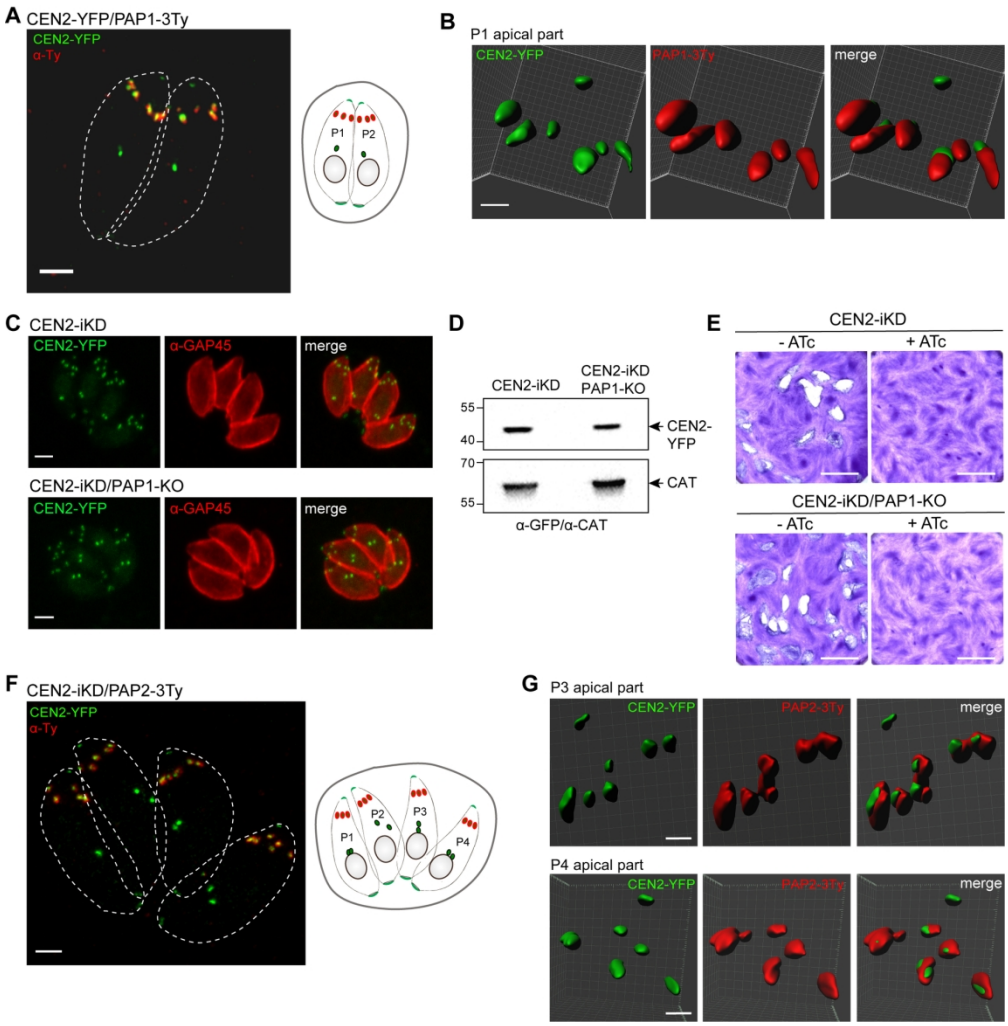

Figure 3

164x174mm (300 x 300 DPI)

Figure 4

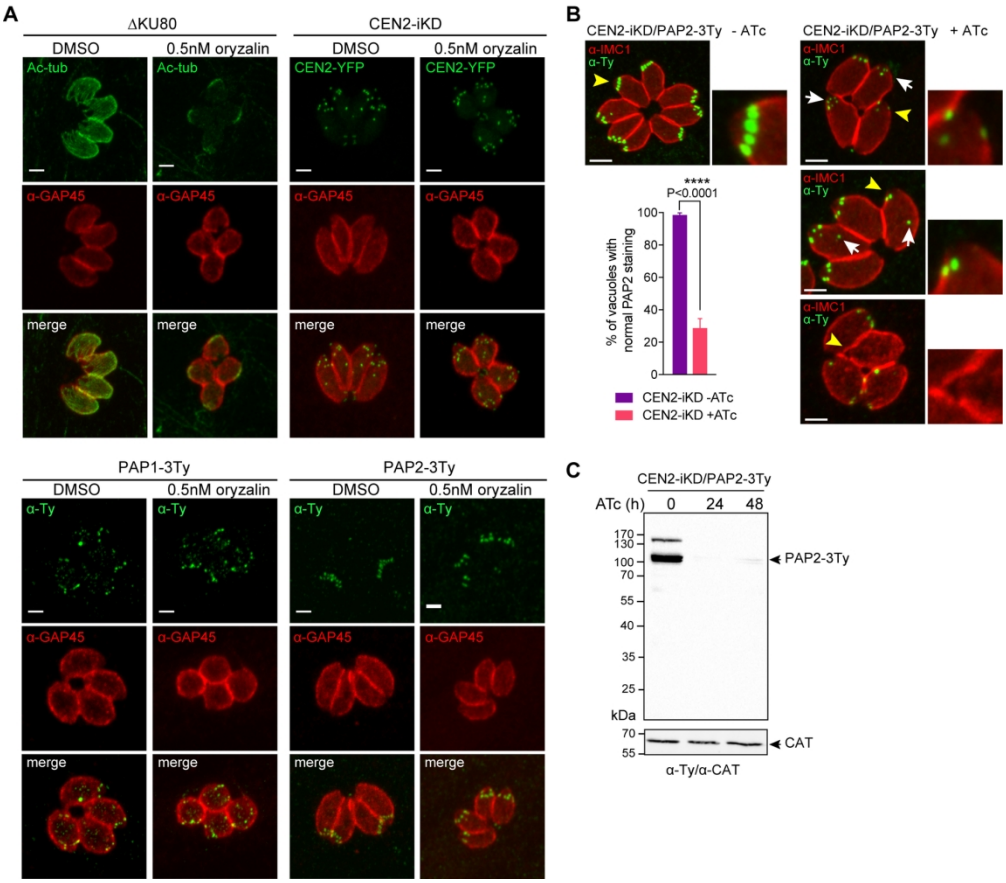

Figure 4

165x150mm (300 x 300 DPI)

Figure 5

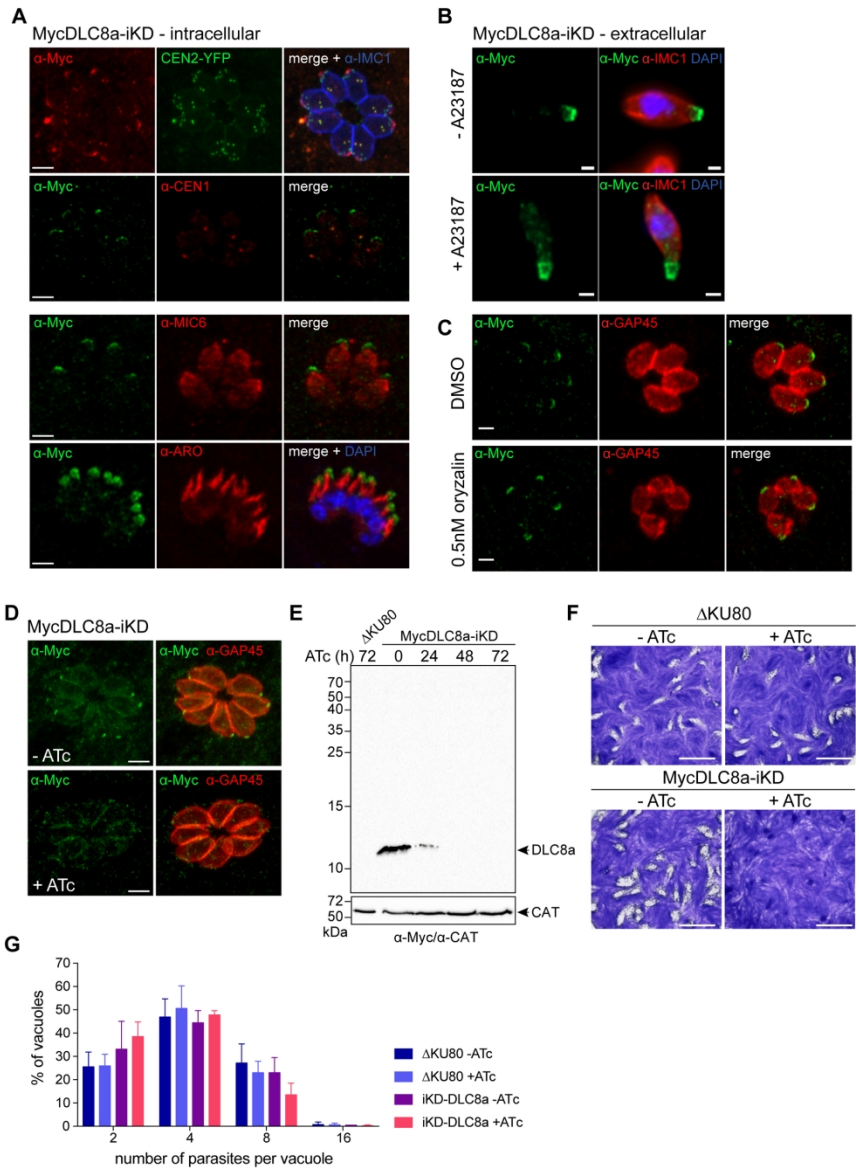

Figure 5

159x224mm (300 x 300 DPI)

Figure 6

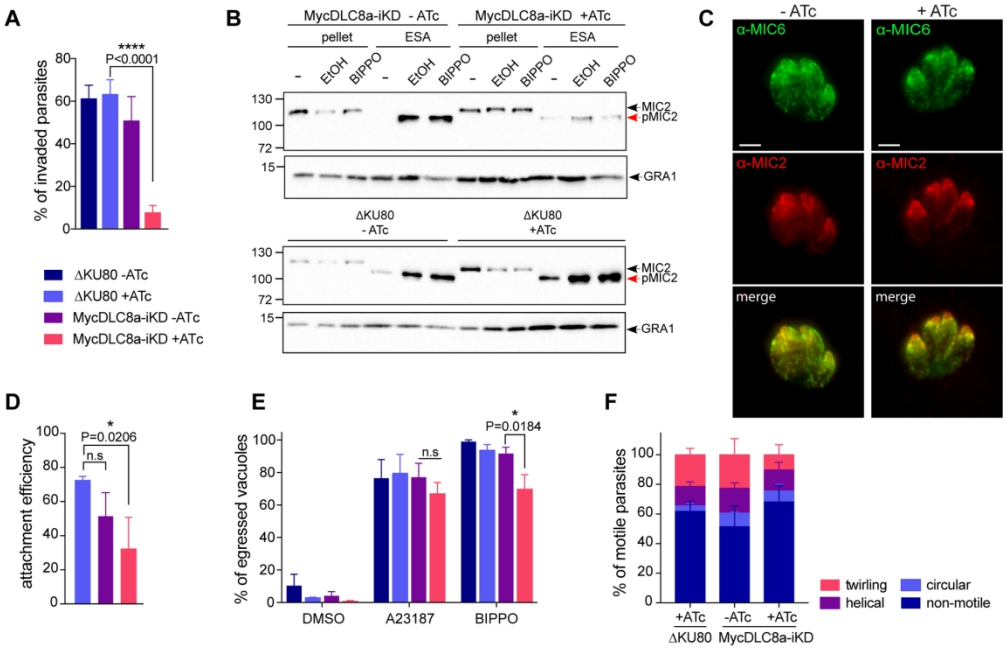

Figure 6

165x113mm (300 x 300 DPI)

Figure 7

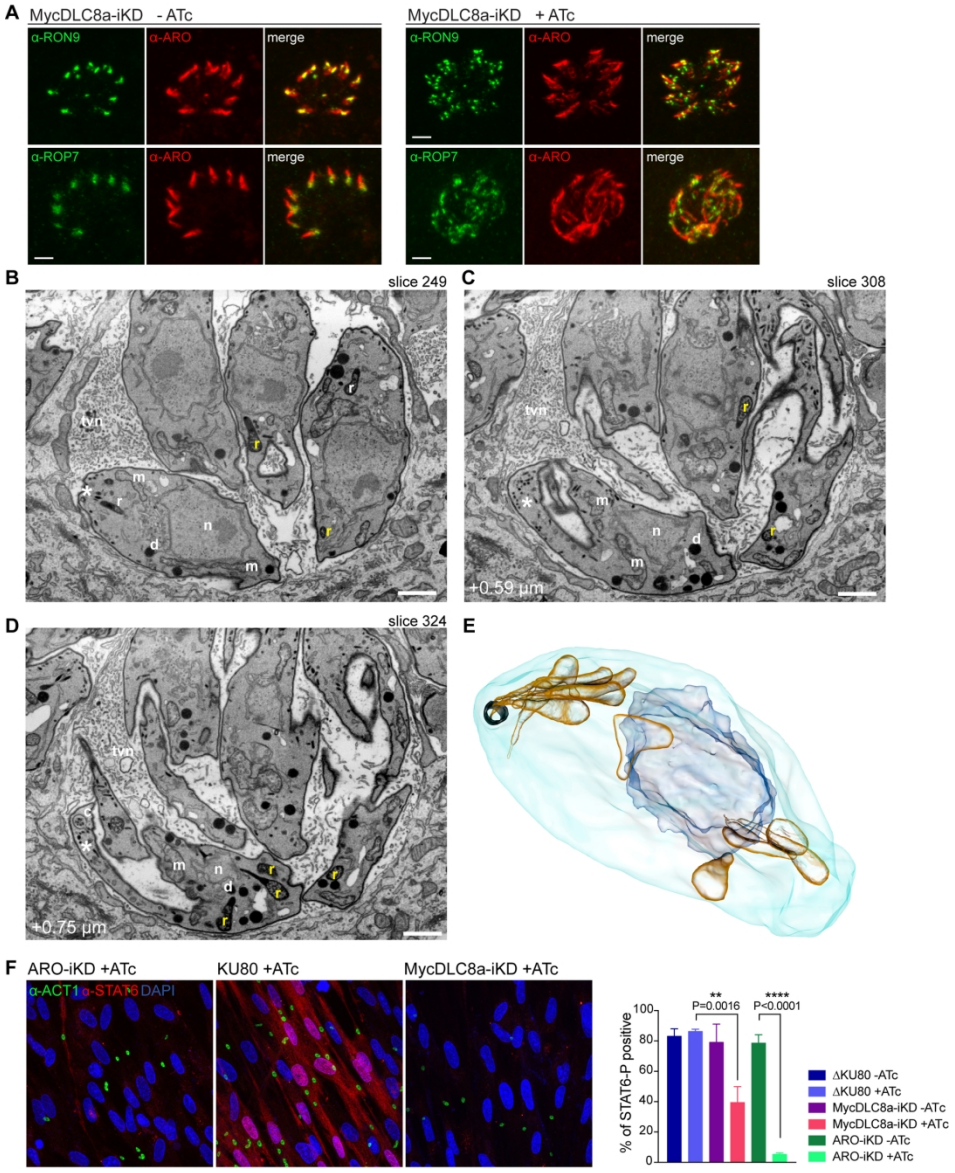

Figure 7

165x209mm (300 x 300 DPI)

Figure 8

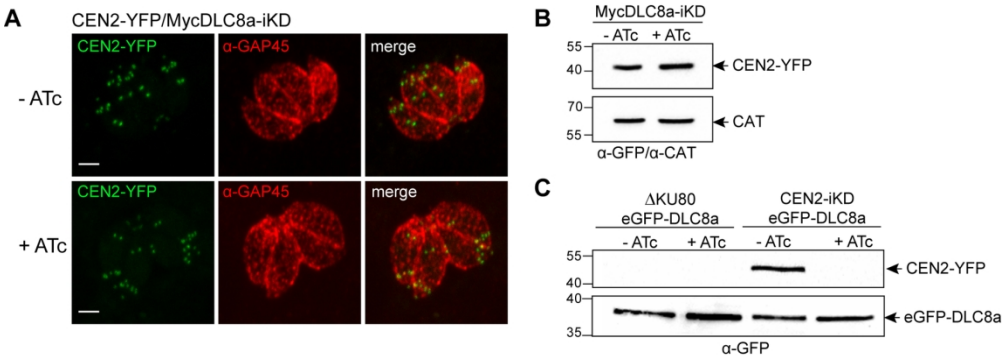

Figure 8

164x65mm (300 x 300 DPI)